



# Cu doped SnS thin films deposited by the spray method: characterization and numerical simulation using SCAPS-1D

A. Rmili<sup>1</sup> · L. Soussi<sup>1</sup> · R. Jdaa<sup>1</sup> · T. Garmim<sup>2</sup> · C. Louardi<sup>3</sup> · A. El Bachiri<sup>3</sup> · A. Louardi<sup>4</sup> · A. Talbi<sup>1</sup> · K. Nouneh<sup>1</sup> · M. Mabrouki<sup>5</sup> · H. Erguig<sup>1</sup>

Received: 17 August 2022 / Accepted: 7 February 2023 / Published online: 17 March 2023  
© The Author(s), under exclusive licence to Springer Science+Business Media, LLC, part of Springer Nature 2023

## Abstract

In this work, the SnS thin film was deposited on the glass substrate by spray technique at 350 °C. The impact of Cu doping on physical properties of the SnS thin film was investigated using a variable doping concentration [Cu/Sn] from 1 to 5%. XRD revealed that films of polycrystalline nature have orthorhombic crystal structures with a preferential orientation along the (111) plane given that peak intensity decreases with increasing Cu doping concentration. Atomic force microscopy and scanning electron microscopy measurements reveal the dependence of surface roughness and morphology because of copper doping. The optical properties were studied by measuring the transmission characteristics which were used to find the optical band gap energy. The Hall effect measurement results confirm the p type of all samples and that their resistivity is strongly dependent on Cu concentration. The influence of the dopant rate on the PV parameters of simulated SnS-based solar cell was studied using the SCAPS-1D software.

**Keywords** SnS thin films · Cu doping · Spray pyrolysis · Opto-electrical properties · SCAPS-1D

---

✉ A. Rmili  
ahmed.rmili@uit.ac.ma

<sup>1</sup> Laboratory of Materials Physics and Subatomic, Ibn Tofail University, Kenitra, Morocco

<sup>2</sup> Laboratory of Condensed Matter Physics (LPMC), Department of Physic, Faculty of Sciences, Chouaib Doukkali University, El-Jadida, Morocco

<sup>3</sup> Bio-Geosciences and Material Engineering Laboratory (LBGIM), Higher Normal School, Hassan II University, Casablanca, Morocco

<sup>4</sup> Laboratory of Industrial Techniques, Department of Industrial Engineering, Faculty of Sciences and Techniques, Sidi Mohamed Ben Abdellah University, Fez, Morocco

<sup>5</sup> University of Sultan Moulay Slimane Faculty of Sciences et Techniques, Beni Mellal, Morocco

## 1 Introduction

Various metal chalcogenide materials have been the subject of a big body of research over the past decades for photovoltaic applications. CdTe, CIGS, CZTS and SnS absorbers have been used in solar cells, and it's been found that the efficiency ranged from 7.68 to 23.4% (Minbashi et al. 2018; Failed 2014; He et al. 2021; Hirai et al. 2013). However, cost-effectiveness and environmental concerns remain important factors in material selection. Tin (II) sulfide has received considerable attention from researchers because Sn and S are abundant naturally on earth and are relatively non-toxic. SnS is a p-type material with a direct energy band gap and a high absorption coefficient (Andrade-Arvizu et al. 2015; Banai et al. 2016; Sinsersuksakul et al. 2014; Koteeswara Reddy et al. 2015; Albers et al. 1961) because of its optimal properties. SnS semiconductors are also found in other various applications such as optoelectronics and gas sensors (Zhu et al. 2014; Nair et al. 2016).

Single-phase orthorhombic SnS films have been elaborated using several techniques, including electrodeposition, spin coating, solvothermal routes, co-evaporation, chemical vapor deposition, and spray (Mariappan et al. 2011; Garmim et al. 2020; Hsu et al. 2015; Robles et al. 2015; Baby et al. 2020a; Mohan et al. 2021). The latter method has advantages that are attributed to its simplicity, the use of low-cost equipment, and controllable thickness of films. Besides, it produces homogeneous and uniform layers with large surfaces. Based on the literature, several works have studied SnS, regarding pure and doped thin films produced by spray pyrolysis, but we think it is still important to understand more the influence of dopant variations on the photovoltaic behavior of the SnS absorber layer.

In this work we aim to elaborate and characterize SnS layers by the simple chemical spray method with the objective of using them in photovoltaic. We also study the effect of doping on some parameters such as the band gap energy, the absorbance, and the conductivity of the SnS thin films. Finally, we propose configuration of solar cells based on thin films using SCAPS software.

## 2 Experimental procedure

### 2.1 Samples preparation

Pure and copper-doped tin sulfide samples were deposited by chemical method using spray pyrolysis technique. The precursor solution was obtained by dissolving tin dichloride dihydrate ( $\text{SnCl}_2 \cdot 2\text{H}_2\text{O}$ ) and thiourea ( $\text{CS}(\text{NH}_2)_2$ ) in 5 ml of distilled water. To this initial solution we added copper chloride ( $\text{CuCl}_2 \cdot 6\text{H}_2\text{O}$ ) with different doping concentrations (0%, 1%, 2%, 3%, 4% and 5%). The resulting solution was vigorously stirred with a magnetic stirrer for 60 min and then manually sprayed onto a glass substrate preheated to 350 °C using a perfume sprayer. Before the deposition process, the glass substrates were cleaned with chlorhydric acid and acetone, then rinsed using deionized water and dried in air. Homemade spray with perfume atomizer has been used successfully to deposit other thin films such as CdS (Ojeda-Barrero et al. 2018),  $\text{Co}_3\text{O}_4$  (Son et al. 2014)  $\text{SnO}_2$  (Wang et al. 2019).

## 2.2 Characterization

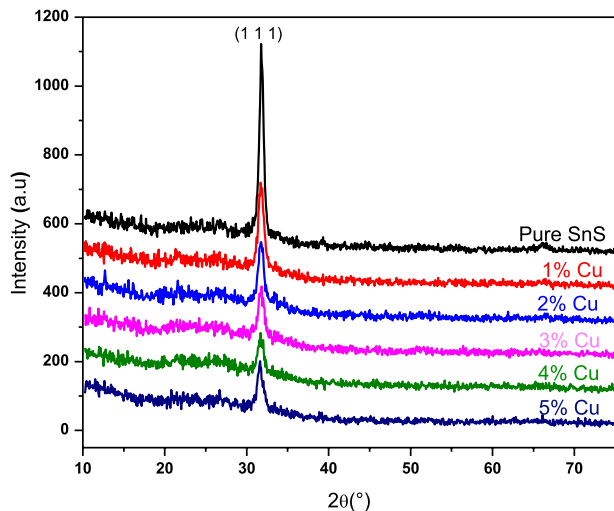
The as-deposited thin films were found to be black in color, non-transparent, uniform, without holes and perfectly adherent to the substrate. The thickness of layers was determined by gravimetric technique, and it was found around 480 nm. The structure, crystallinity and phase of pure and copper-doped tin sulphide samples were determined using X-ray diffraction (XRD) analysis (XPRT-PRO) model using  $\text{CuK}\alpha$  radiation ( $\lambda = 1.542 \pm 0.002 \text{ \AA}$ ) with  $2\theta$  ranging from  $15^\circ$  to  $80^\circ$ . The surface morphology of samples was characterized by scanning electron microscopy (SEM) (Model: Quattro, Thermo Fisher Scientific) and by atomic force microscopy (AFM) (Nanosurf Easyscan). Optical transmittance measurements were carried out by means of a UV-Vis-NIR spectrophotometer (SHIMADZU 3101 PC) in the wavelength range of 300–2500 nm, and electrical studies of the films were performed at room temperature using a LINSEIS, HCS1-hall effect measurement system.

## 3 Results and discussion

### 3.1 Structural analysis

X-ray diffractograms of pure and copper doped SnS samples with doping concentrations: 1%, 2%, 3% 4% and 5% are depicted in Fig. 1. These spectra show a single diffraction peak at position  $2\theta = 31.78^\circ$ , corresponding to the (111) diffraction plane. The comparison of the inter-reticular distance  $d_{hkl}$  with standard reference values (JCPDS card N 01-073-1859) confirms that all these thin films crystallize in the orthorhombic structure of SnS. This indicates that the crystal structure has not been affected by Cu doping which suggests that the  $\text{Cu}^{2+}$  doping ions are incorporated into the SnS structure in a substitutional manner by replacing the  $\text{Sn}^{2+}$  ion sites. Moreover, no additional secondary phases were observed such as  $\text{Sn}_2\text{O}_3$ ,  $\text{SnS}_2$ ,  $\text{SnO}_2$ ,  $\text{CuS}$  or  $\text{CuO}$  which could influence physical or optical properties of our thin films. Other works indicate the appearance of  $\text{Sn}_2\text{O}_3$  and  $\text{SnS}_2$  in the SnS

**Fig. 1** XRD patterns of pure and Cu-doped SnS thin films



films independently of the deposition method used (Minbashi et al. 2018; Mariappan et al. 2011).

All thin films show the preferred orientation along the [111] direction. The peak intensity of the (111) plane decreased with increasing Cu dopant concentration, indicating a slight improvement of the crystal quality of SnS films. This is probably due to the formation of novel nucleation centers by the incorporation of Cu. It is reported that the maximum efficiency for SnS based solar cell is generally noted for the planar-oriented (111) SnS films (Baby et al. 2020b).

The crystallite sizes ( $D_{hkl}$ ) of Cu-doped SnS were calculated using the X-ray diffraction patterns by the Scherrer formula Eq. (1) (Kadam and Patil 2001), the strain  $\varepsilon$  was founded using Eq. (2) (Begum et al. 2012), and dislocation density established by Eq. (3) (Islam et al. 2013). Where  $\lambda$  is the incident radiation wavelength ( $\lambda = 1.542 \text{ \AA}$ ),  $\beta_{hkl}$  is the width of the half-maximum of the hkl line and  $\theta_{hkl}$  is the Bragg angle. Table 1 shows the values obtained.

$$D_{hkl} = 0.9 \frac{\lambda}{\beta_{hkl} \cos \theta_{hkl}} \quad (1)$$

$$\varepsilon = \left( \frac{1}{\sin \theta} \right) \left[ \left( \frac{\lambda}{D} \right) - \beta \cos \theta \right] \quad (2)$$

$$\delta = \frac{1}{D^2} \quad (3)$$

From Table 1 the  $D_{hkl}$  crystallite size varies with Cu-doped concentration and reaches a maximum value of 36.37 nm for 5% doped SnS thin films. A similar result was given by Thangaraju and Kaliannan (2000) for SnS films elaborated by spray method on glass substrates at temperature 350 °C and Bommireddy et al. (2017) for Cu-doped SnS semiconductor grown by Sol–Gel. The dislocation density  $\delta$  and strain  $\varepsilon$  generally vary inversely compared to the  $D_{hkl}$  crystallite sizes.

### 3.2 Surface morphology

The study of the morphology of undoped and Cu-doped SnS thin films was investigated by scanning electron microscopy (SEM) and atomic force microscopy (AFM). Figure 2

**Table 1** Different structural parameters calculated from the XRD data

Sample	$2\theta$ (°)	FWHM (2 $\theta$ )	d-spacing (Å)	$D_{hkl}$ (nm)	Microstrain $\varepsilon$	Dislocation density $\delta$ ( $10^{15}$ lignes/m <sup>2</sup> )
<i>Pure and Cu doped SnS</i>						
0%	31.79	0.461	2.814	20.37	0.691	2.410
1%	31.79	0.643	2.812	11.44	1.229	7.640
2%	31.67	0.329	2.825	28.77	0.491	1.209
3%	31.73	0.659	2.819	14.18	0.994	4.973
4%	31.78	0.964	2.813	7.42	1.896	18.16
5%	31.65	0.264	2.827	36.37	0.388	0.756

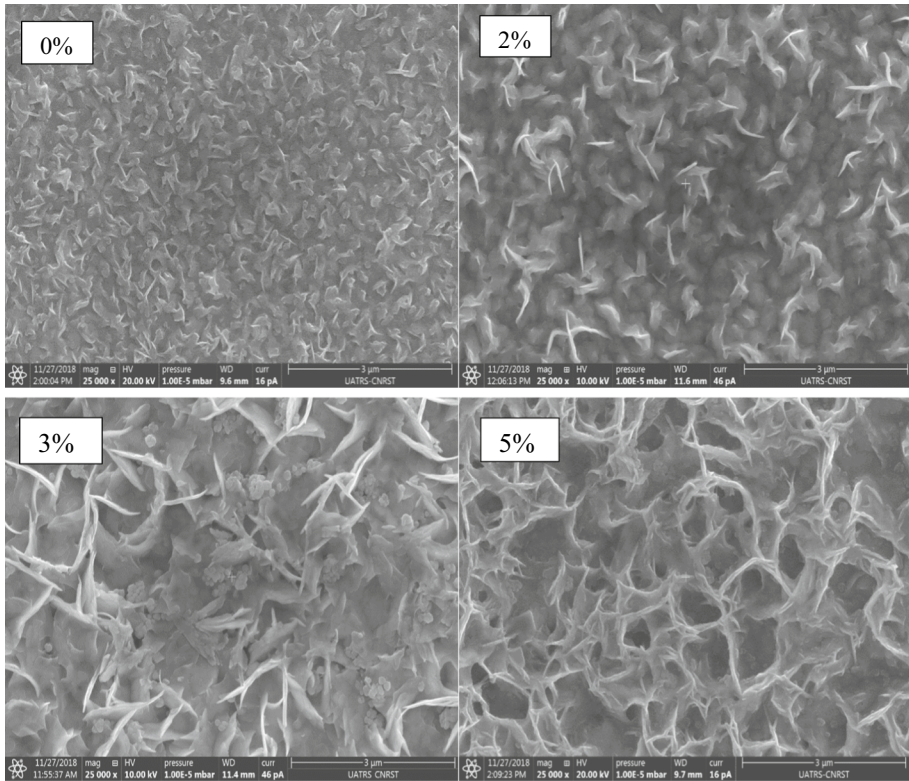


**Fig. 2** SEM images of SnS samples with 0%, 2%, 3% and 5% of Cu

shows the SEM images obtained for the Cu-doped SnS samples with different Cu doping concentrations. We notice that all the thin films present a dense and homogeneous surface with flower-like grains. From these images, we can deduce that the Cu doping influences the morphology of the thin films. In this case, the size of the grains varies according to the concentration of the Cu doping.

Figure 3 shows the 2D AFM images of Cu doped SnS films. These AFM images indicate that the surface roughness (RMS) and particle size of Cu doped SnS films depend also on the Cu doping concentrations. The particle size rises with increasing the Cu doping concentrations which is in good agreement with the results already obtained by scanning electron microscopy (SEM).

### 3.3 Optical study

The optical transmission spectra of SnS samples prepared at different Cu doping rate are illustrated in Fig. 4. As can be seen, all thin films show low optical transmission not exceeding 15% in the UV and visible region due to the strong absorption in the UV–Visible. The high absorption coefficient indicated that the SnS thin films can be used as an absorber layer in solar cells (Gedi et al. 2015). We note that the optical transmission of Cu-doped SnS thin films rises with Cu doping concentration. This finding may be a result of

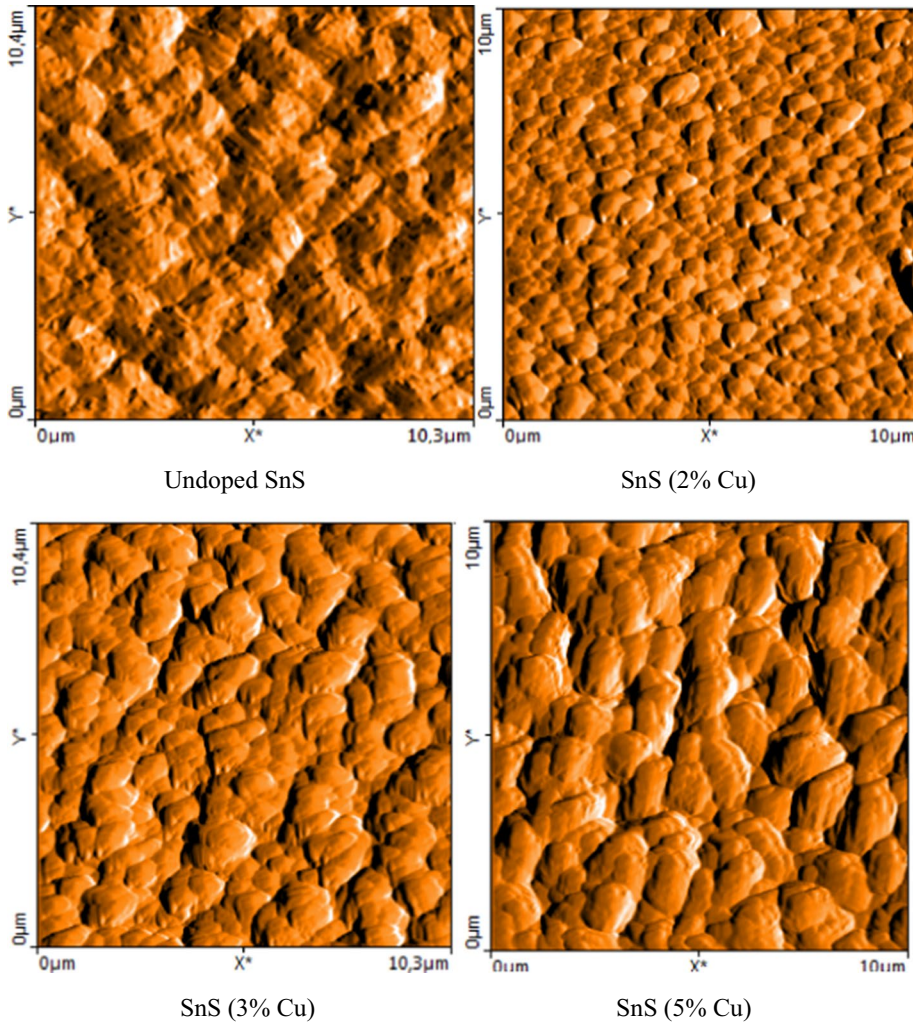


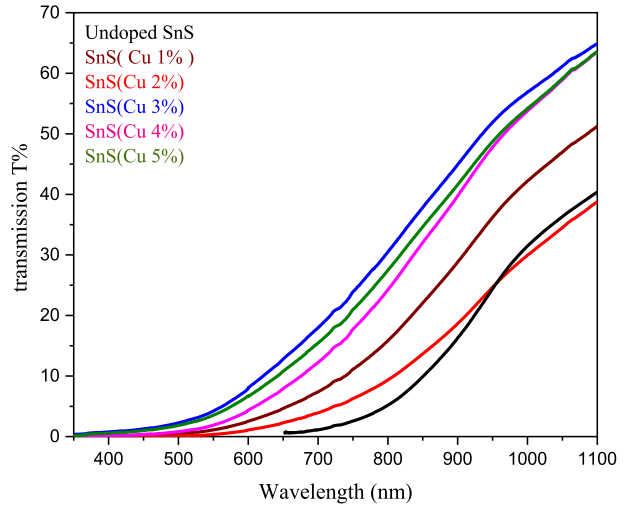
**Fig. 3** AFM images of undoped and SnS:Cu films with different Cu concentrations

the substitution of  $\text{Sn}^{2+}$  ion by  $\text{Cu}^{2+}$ . We also note that the absorption edge shifts with Cu doping towards the short wavelengths.

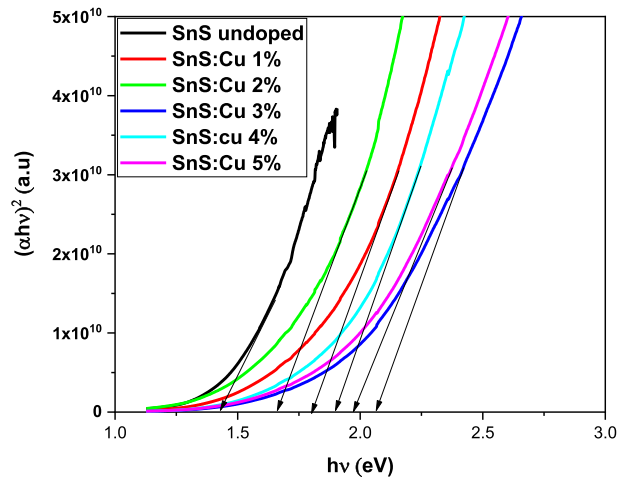
Figure 5 shows the curves of  $(\alpha h\nu)^2$  versus  $(h\nu)$  for undoped and Cu doped SnS layers. We observe that Cu doping causes an increase in the band gap energy  $E_g$  from 1.46 to 1.98 eV. Indeed, this increase was attributed to the variation of the crystallite size, disorder at grain boundaries and structural defects following the incorporation of Cu doping atoms. Similar observations have been previously reported for Cu-doped SnS films growth by thermal evaporation method (Lavanya et al. 2022). The values of the optical gap energy  $E_g$  are presented in Table 2.

Figure 6 depicts the coefficient absorption variation as a function of the wavelength for Cu-doped SnS films. This figure confirmed that the SnS has high absorption in the visible range. It is also deduced from this figure that the absorption values decrease with the

**Fig. 4** Optical transmission curves of undoped and doped SnS at different Cu concentrations



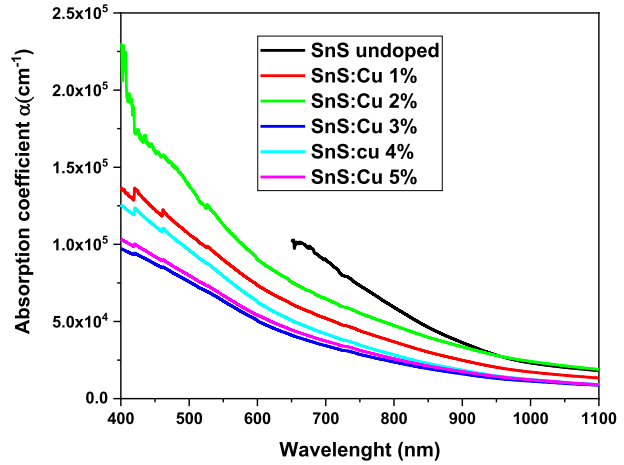
**Fig. 5**  $(\alpha h\nu)^2$  with  $h\nu$  of SnS layers with different Cu doping concentrations



**Table 2** Values of optical gap energy  $E_g$  and absorption coefficient of Cu doped SnS

Sample	$E_g$ (eV)	$\alpha \times 10^4$ (cm <sup>-1</sup> )
SnS:Cu 0%	1.46	3.57
SnS:Cu 1%	1.85	3.62
SnS:Cu 2%	1.67	4.65
SnS:Cu 3%	2.08	2.32
SnS:Cu 4%	1.93	2.69
SnS:Cu 5%	1.98	2.45

**Fig. 6** Absorption coefficient of pure and doped SnS at different Cu concentrations



incorporation of Cu, especially when the doping ratios become greater than 2%. This may be attributed to the degradation of Cu or to the insertion of more Cu atoms caused by the distortion of the SnS structure (Garmim et al. 2021).

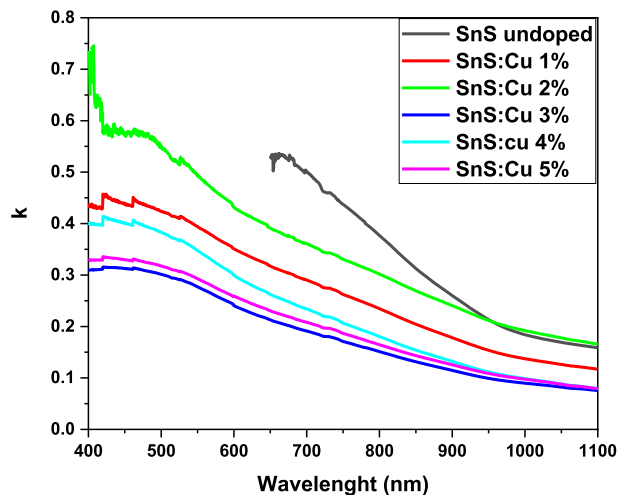
The extinction coefficient of Cu doped SnS samples is determined from the absorption coefficient using the following equation (Garmim et al. 2020).

$$k = \frac{\alpha\lambda}{4\pi} \tag{4}$$

Figure 7 shows the extinction coefficient variation for undoped and Cu doped SnS thin films. A decrease in  $k$  when increasing the wavelength is noticed in this figure. In addition, the extinction coefficient is directly proportional to the absorption coefficient. So, the variation behavior of  $k$  as a function of the Cu-incorporation is the same as that of the absorption coefficient.

The optical refractive index is determined from reflectance and extinction coefficient using the ensuing equation (Garmim et al. 2020):

**Fig. 7** Extinction coefficient of undoped and doped SnS at different Cu concentrations





$$n = \left( \frac{1+R}{1-R} \right) + \sqrt{\frac{4R}{(1-R)^2} - k^2} \quad (5)$$

The variation of refractive index for Cu doped SnS thin films is shown in Fig. 8. The high values of refractive index of our films are mainly due to the strong absorbance of SnS. In addition, the prepared films at high density give a high refractive index, this is confirmed by MEB and AFM analysis. The decrease in the refractive index values with increasing wavelength attributes to scattering behavior normal.

The permittivity dielectric constant is an intrinsic parameter to understand the optical behavior of material. It is mainly related to the refractive index "n" and the extinction coefficient "k" by the above relation (Garmim et al. 2020):

$$\varepsilon = (n^2 - k^2) + (2nk) = \varepsilon_r + i\varepsilon_i \quad (6)$$

Figures 9 and 10 show the real and imaginary part of dielectric constant, respectively. We can remark that the real and imaginary part decrease as the wavelength increases for both undoped and Cu doped SnS films. In addition, the Cu insertion in SnS causes an increase of the dielectric parameters. This may have a link with the increase in particle size with incorporation of Cu with different ratios.

### 3.4 Electrical properties

Resistivity, Mobility and Carrier concentration performed by Hall-Effect are tabulated in Table 3, we noticed that the elaborated films have P type conductivity. Increasing the doping rate from 0 to 2%, increases the charge carrier density of films and decrease the resistivity and the mobility to 0.1881  $\Omega$  cm and 8.99  $\text{cm}^2/\text{V/S}$  respectively. This may be a consequence of the increase in acceptor sites due to the occupation of Cu ions in the substitution sites. However, starting from Cu concentration 3% the resistivity of the layers progressively increases. This may be a result of the decrease in the carrier lifetime due to the increase in grain boundaries when the dopant concentration is increased in agreement with other studies (Bommireddy et al. 2017).

**Fig. 8** Refractive index of undoped and doped SnS at different Cu concentrations

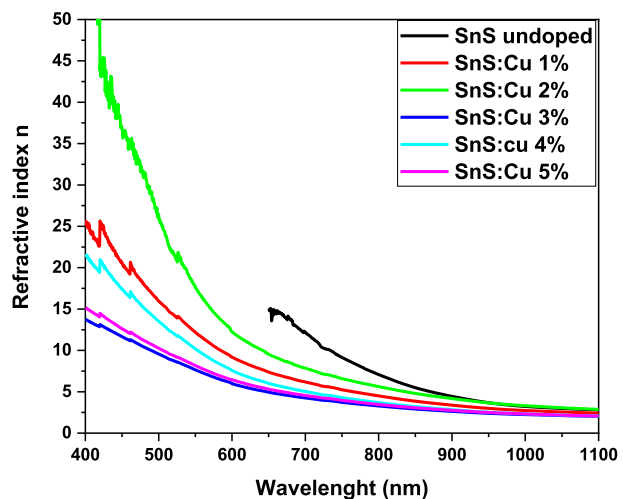


**Fig. 9** Real part of dielectric constant of pure and doped SnS at different Cu concentrations

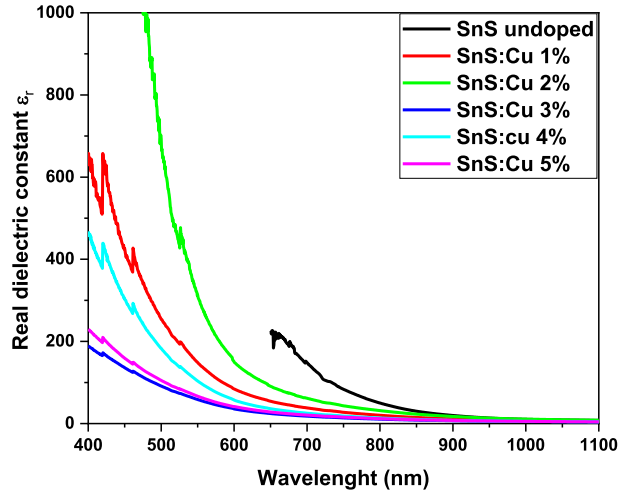


**Fig. 10** Imaginary part of dielectric constant of pure and doped SnS at different Cu concentrations

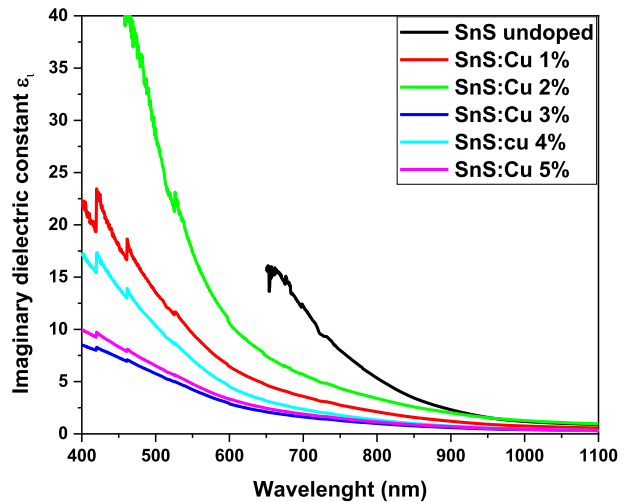


**Table 3** Hall effect measurement results of Cu doped SnS in room temperature

Parameters	Resistivity $\rho$ ( $\Omega\text{cm}$ )	Hall coefficient $R_H$ ( $\text{cm}^3/\text{C}$ )	Mobility $\mu_H$ ( $\text{cm}^2/\text{V/s}$ )	Carrier concentration ( $\text{cm}^{-3}$ )	Type of conduction
Pure SnS	0.2851	22.74	79.73	$2.745 \cdot 10^{17}$	P
SnS:Cu 1%	0.2444	6.294	25.75	$9.917 \cdot 10^{17}$	P
SnS:Cu 2%	0.1881	1.691	8.991	$3.690 \cdot 10^{18}$	P
SnS:Cu 3%	0.3506	20.88	51.15	$3.670 \cdot 10^{17}$	P
SnS:Cu 4%	0.3595	21.98	61.13	$2.840 \cdot 10^{17}$	P
SnS:Cu 5%	0.3655	32.13	87.91	$1.943 \cdot 10^{17}$	P

## 4 Simulation results

SCAPS-1D (solar cell capacitance simulator) is a numerical simulation software for heterojunction thin films solar cells. It has been developed at the University of Gent in Belgium with LabWindows by Niemegeers et al. (2013). This software solves the equations of structures containing several layers of semiconductors with arbitrary doping profile and arbitrary energy distribution of deep acceptor and donor levels under different sources of illumination. Iterations of equation solving are done until the algorithm converges. SCAPS 1-D was introduced in the literature (Niemegeers et al. 1996; Burgelman et al. 2000). While SCAPS algorithms are detailed in reference (Niemegeers et al. 1998). The use of SCAPS is very practical, it allows to simulate any photovoltaic structure, according to the materials available in data files, varying the parameters such as width, surface, doping, etc. (Niemegeers and Burgelman 1997; Burgelman et al. 1999). Generally, the study of semiconductors is based on the simultaneous resolution of the three equations: Poisson's Eq. (4), the continuity equation for electrons (5) and for holes (6).

$$\frac{d^2\Psi(x)}{dx^2} = \frac{e}{\epsilon_0\epsilon_r}(p(x) - n(x) + N_D - N_A + \rho_p - \rho_n) \quad (7)$$

$$\frac{d}{dx}J_n(x) - e\frac{\partial n(x)}{\partial t} - e\frac{\partial \rho_n}{\partial t} = G(x) - R(x) \quad (8)$$

$$\frac{d}{dx}J_p(x) - e\frac{\partial p(x)}{\partial t} - e\frac{\partial \rho_p}{\partial t} = G(x) - R(x) \quad (9)$$

With  $\Psi$  is the electric potential,  $\epsilon_r$  relative permittivity,  $\epsilon_0$  vacuum permittivity,  $e$  the electrical charge of the electron,  $p$  and  $n$  concentrations of holes and electrons,  $N_A$  and  $N_D$  are respectively the charge carrier densities of acceptor and donor impurities,  $J_p$  and  $J_n$  the densities of hole and electron currents,  $\rho_p$  and  $\rho_n$  the distributions of holes and electrons,  $G(x)$  and  $R(x)$  the generation and recombination charge (Movla 2014; Simya et al. 2015).

In the current section, we proposed a device of a solar cell based on SnS doped with Cu in the form Cu:SnS/CdS/SnO<sub>2</sub>. The schematic representation of the studied heterojunction is shown in Fig. 11. Here, the simulation parameter values of buffer layer CdS

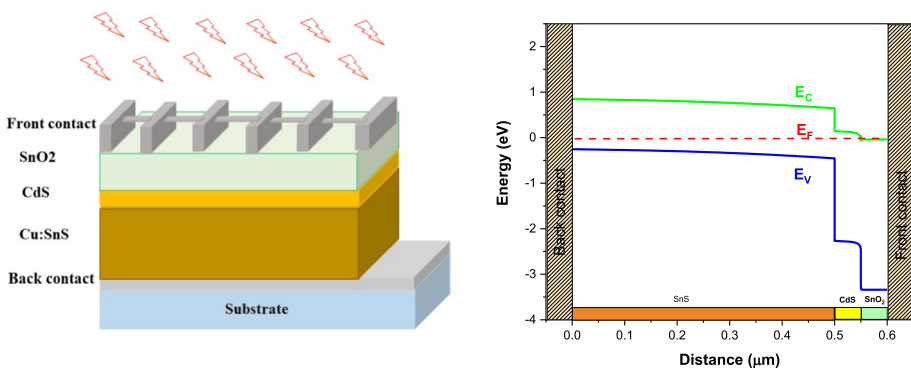
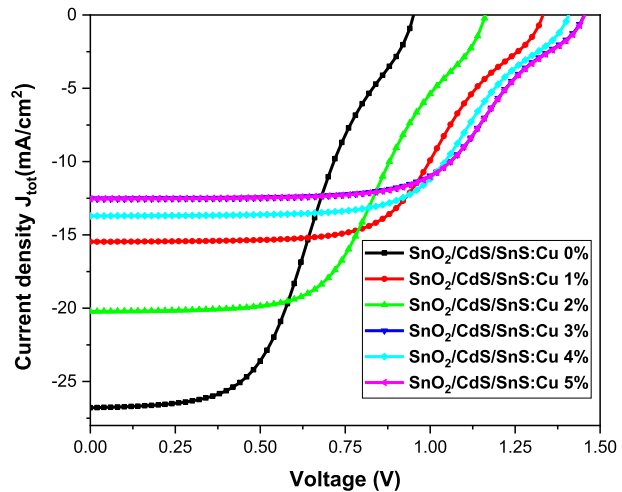


Fig. 11 Schematic diagram of a conventional Cu:SnS/CdS/SnO<sub>2</sub> photovoltaic device

**Table 4** Parameters of the semiconductors used for the SnS/CdS/SnO<sub>2</sub> solar cell (Minbashi et al. 2018; Garmim et al. 2022)

Films	SnO <sub>2</sub>	CdS	SnS
Thickness (μm)	0.05	0.05	0.5
Band gap (eV)	3.6	2.45	Varied [exp]
Electron affinity (eV)	4.6	4.4	4.07
Dielectric permittivity	9	10	Varied [exp]
CB effective density of states (/cm <sup>3</sup> )	2.2 × 10 <sup>18</sup>	1.8 × 10 <sup>19</sup>	2.2 × 10 <sup>19</sup>
VB effective density of states (/cm <sup>3</sup> )	1.8 × 10 <sup>19</sup>	2.4 × 10 <sup>19</sup>	5.5 × 10 <sup>20</sup>
Electron thermal velocity (cm/s)	1 × 10 <sup>7</sup>	1 × 10 <sup>7</sup>	1 × 10 <sup>7</sup>
Hole thermal velocity (cm/s)	1 × 10 <sup>7</sup>	1 × 10 <sup>7</sup>	1 × 10 <sup>7</sup>
Electron mobility (cm <sup>2</sup> /VS)	100	35	80
Hole mobility (cm <sup>2</sup> /VS)	25	50	0.1
Shallow uniform donor density ND (/cm <sup>3</sup> )	1 × 10 <sup>20</sup>	1 × 10 <sup>17</sup>	0
Shallow uniform acceptor density NA (/cm <sup>3</sup> )	0	0	1 × 10 <sup>16</sup>

**Fig. 12** J–V Characteristic of SnO<sub>2</sub>/CdS/SnS:Cu solar cell

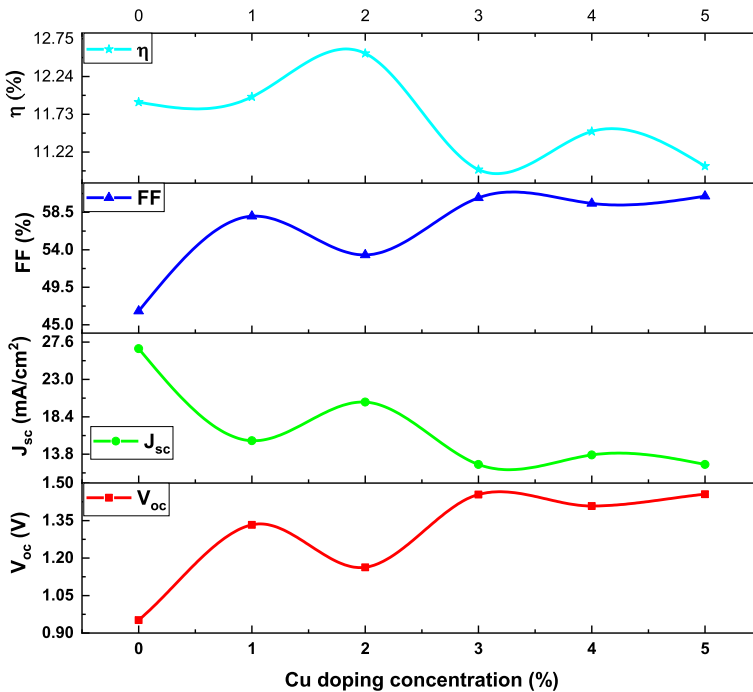


and window layer SnO<sub>2</sub> are introduced from literature which are listed in Table 4. However, for the undoped and Cu-doped SnS layer, the simulation values were experimentally extracted such as E<sub>g</sub>, dielectric permittivity, absorption coefficient and carrier concentration.

Figure 12 shows the J–V characteristic of the SnS/CdS/SnO<sub>2</sub> solar cell. The simulation results of this solar cell indicate that the conversion efficiency improved from 10.98, to 12.55% indicating that Cu-doped SnS is a good absorbent material for photovoltaic applications. We tested the effect of varying the Cu dopant concentration on the open-circuit voltage (V<sub>oc</sub>), short-circuit current (J<sub>sc</sub>), fill factor (FF) and efficiency. Table 5 and Fig. 13 show the PV parameters of the simulated SnS/CdS/SnO<sub>2</sub> solar cell. We notice that V<sub>oc</sub> increases with increasing dopant when the concentration exceeds 3% Cu. Here, we can see from Fig. 13 an important improvement in efficiency with adding of Cu from 1 to 2%. This is attributed to the decreasing of band gap energy, which makes SnS to absorb

**Table 5** PV parameters of simulated SnO<sub>2</sub>/CdS/SnS:Cu solar cell

	V <sub>oc</sub> (V)	J <sub>sc</sub> (mA/cm <sup>2</sup> )	FF (%)	η (%)
SnO <sub>2</sub> /CdS/SnS:Cu 0%	0.95	26.79	46.64	11.89
SnO <sub>2</sub> /CdS/SnS:Cu 1%	1.33	15.46	58.03	11.96
SnO <sub>2</sub> /CdS/SnS:Cu 2%	1.16	20.22	53.38	12.55
SnO <sub>2</sub> /CdS/SnS:Cu 3%	1.45	12.53	60.24	10.98
SnO <sub>2</sub> /CdS/SnS:Cu 4%	1.40	13.70	59.56	11.49
SnO <sub>2</sub> /CdS/SnS:Cu 5%	1.45	12.53	60.43	11.02

**Fig. 13** Variation of SnO<sub>2</sub>/CdS/SnS:Cu solar cell parameters by doping concentration

strongly and leads more charge generation. Overall, the best-obtained value for  $\eta$  in this case is 12.55% corresponding to  $E_g = 1.67$  eV for Cu-doped SnS with ratio equal to 2%.

## 5 Conclusion

In summary, we have successfully elaborated the Cu doped SnS thin films using a simple and inexpensive technique (spray), and we have studied some of their properties. The XRD showed that the prepared films are polycrystalline with an orthorhombic structure and a preferential orientation along [111] direction while the crystallite size varies with the dopant concentration. The analysis of surface morphology by SEM and AFM microscopy,

showed that SnS:Cu thin films have a homogeneous uniform surface and adhere well to the substrate. The optical measurements illustrate that the SnS thin films are opaque with a very low optical transmission and a high absorption in the visible domain. A slight increase of the transmission is observed with the incorporation of Cu in the SnS layers. We found that the optical gap energy increased from 1.46 to 1.98 eV, when the copper concentration increased from 0 to 5%. Yet, the absorption coefficient takes values higher than  $10^4 \text{ cm}^{-1}$ . Using SCAPS-1D software, we studied, by simulation, the effect of Cu doping on the performance of the SnO<sub>2</sub>/CdS/SnS:Cu solar cell. We noticed that the parameters of the cell such as Voc, Jsc, FF and  $\eta$  vary when the concentration of the Cu changes. We arrived at the conclusion that a good performance is found in films doped 2% Cu because of the crystalline qualities, low resistivity, and optimal gap energy, which shows that this material can be used as a potential absorbing thin film in solar cells.

**Acknowledgements** We thank Professor Marc Burgelman of Ghent University for the development of the SCAPS-1D simulation software.

**Authors' contributions** AR and LS: Writing—original draft, Investigation, Conceptualization. RJ and TG: Investigation, Prepare figures. AT and KN: Methodology, Validation. AEB and CL: Conceptualization, Review. AL and MM: Prepare figures, Review and editing. HE: Validation, Supervision.

**Funding** Not applicable.

**Availability of data and materials** There is no availability of data.

## Declarations

**Conflict of interest** The authors declare that they have no known competing financial interests or personal relationships that could have appeared to influence the work reported in this paper.

**Ethical approval** Not applicable.

## References

- Albers, W., Haas, C., Vink, H.J., Wasscher, J.D.: Investigations on SnS. *J. Appl. Phys.* **32**, 2220–2225 (1961). <https://doi.org/10.1063/1.1777047>
- Andrade-Arvizu, J.A., Courel-Piedrahita, M., Vigil-Galan, O.: SnS-based thin film solar cells: perspectives over the last 25 years. *J. Mater. Sci. Mater. Electron.* **26**, 4541–4556 (2015). <https://doi.org/10.1007/s10854-015-3050-z>
- Baby, B.H., Amrutha, E.G., Mohan, D.B.: The formation of orthorhombic SnS nanorods using CTAB in solvothermal method with its phase stability, optical and electrical properties. *Mater. Res. Bull.* **128**, 110883 (2020a). <https://doi.org/10.1016/j.materresbull.2020.110883>
- Baby, B.H., Thomas, A.M., Amrutha, E.G., Mohan, D.B.: Enhancement of optoelectronic properties via substitutional doping of Cu, in and Ag in SnS nanorods for thin film photovoltaics. *Solar Energy* **205**, 446–455 (2020b). <https://doi.org/10.1016/j.solener.2020.05.076>
- Banai, R.E., Horn, M.W., Brownson, J.R.S.: A review of tin (II) monosulfide and its potential as a photovoltaic absorber. *Sol. Energy Mater. Sol. Cells* **150**, 112–129 (2016). <https://doi.org/10.1016/j.solmat.2015.12.001>
- Begum, A., Hussain, A., Rahman, A.: Effect of deposition temperature on the structural and optical properties of chemically prepared nanocrystalline lead selenide thin films. *J. Nanotechnol.* **3**, 438–443 (2012). <https://doi.org/10.3762/bjnano.3.50>
- Bommireddy, P.R., Musalikunta, C.S., Uppala, C., Park, S.H.: Influence of Cu doping on physical properties of sol-gel processed SnS thin Films. *Mater. Sci. Semicond. Process.* **71**, 139–144 (2017). <https://doi.org/10.1016/j.mssp.2017.07.020>

- Burgelman, M., Nollet, P., Degrave, S.: Electronic behaviour of thin-film CdTe solar cells. *Appl. Phys. A* **69**, 149–153 (1999)
- Burgelman, M., Nollet, P., Degrave, S.: Modelling polycrystalline semiconductor solar cells. *Thin Solid Films* **361**, 527–532 (2000). [https://doi.org/10.1016/S0040-6090\(99\)00825-1](https://doi.org/10.1016/S0040-6090(99)00825-1)
- Garmim, T., Chahib, S., Soussi, L., Mghaiouini, R., El Jouad, Z., Louardi, A., Karzazi, O., El Jouad, M., Hlil, E.K., Hartiti, B., Monkade, M.: Optical, electrical, and electronic properties of SnS thin films deposited by sol gel spin coating technique for photovoltaic applications. *J. Mater. Sci. Mater. Electron.* **31**, 20730 (2020). <https://doi.org/10.1007/s10854-020-04586-y>
- Garmim, T., Bouabdalli, E., Soussi, L., El Jouad, Z., Mghaiouini, R., Louardi, A., Hartiti, B., El Jouad, M., Monkad, M.: Opto-electronic properties of Ni and Mg co-doped CdS thin films prepared by spin coating technique. *Phys. Scr.* **96**, 045813 (2021). <https://doi.org/10.1088/1402-4896/abe3c0>
- Garmim, T., Benaiss, N., Soussi, L., Mghaiouinia, R., Bouabdalli, E., Chahid, E., El Jouad, Z., Louardi, A., Hartiti, B., Monkade, M.: Effect of alternative buffer layers for SnS based solar cells: numerical analysis using SCAPS-1D. *Mater. Today Proc.* (2022). <https://doi.org/10.1016/j.matpr.2022.04.289>
- Gedi, S., Minnam Reddy, V.R., Park, C., Wook, J.C., Ramakrishna Reddy, K.T.: Comprehensive optical studies on SnS layers synthesized by chemical bath deposition. *Opt. Mater.* **42**, 468–475 (2015). <https://doi.org/10.1016/j.optmat.2015.01.043>
- He, F., Li, J., Lin, S., Long, W., Wu, L., Hao, X., Zhang, J., Feng, L.: Semitransparent CdTe solar cells with CdCl<sub>2</sub> treated absorber towards the enhanced photovoltaic conversion efficiency. *Sol. Energy* **214**, 196–204 (2021). <https://doi.org/10.1016/j.solener.2020.11.049>
- Hirai, Y., Kurokawa, Y., Yamada, A.: Numerical study of Cu(In, Ga)Se<sub>2</sub> solar cell performance toward 23% conversion efficiency. *Jpn. J. Appl. Phys.* **53**, 012301–012305 (2013). <https://doi.org/10.7567/JJAP.53.012301>
- Hsu, H.T., Chiang, M.H., Huang, C.H., Lin, W.T., Fu, Y.S., Guo, T.F.: Effects of Ge- and Sb-doping and annealing on the tunable bandgaps of SnS films. *Thin Solid Films* **584**, 37–40 (2015). <https://doi.org/10.1016/j.tsf.2014.10.065>
- Islam, M.A., Hossain, M.S., Aliyu, M.M., Karim, M.R., Razykov, T., Sopian, K., Amin, N.: Effect of CdCl<sub>2</sub> treatment on structural and electronic property of CdTe thin films deposited by magnetron sputtering. *Thin Solid Films* **546**, 367–374 (2013). <https://doi.org/10.1016/j.tsf.2013.04.067>
- Kadam, L.D., Patil, P.S.: Thickness-dependent properties of sprayed cobalt oxide thin films. *Mater. Chem. Phys.* **68**, 225–232 (2001). [https://doi.org/10.1016/S0254-0584\(00\)00367-9](https://doi.org/10.1016/S0254-0584(00)00367-9)
- Koteeswara Reddy, N., Devika, M., Gopal, E.S.R.: Review on tin (II) sulfide (SnS) material: synthesis, properties, and applications. *Crit. Rev. Solid State Mater. Sci.* **40**, 359–398 (2015). <https://doi.org/10.1080/10408436.2015.1053601>
- Lavanya, S., Rajesh Kumar, T., Vimala Juliet, A., Hakami, J., Ashraf, I.M.: Noticeable photo-sensing properties of SnS: Cu thin films fabricated by thermal evaporation technique. *Solid State Sci.* **128**, 106889 (2022). <https://doi.org/10.1016/j.solidstatesciences.2022.106889>
- Mariappan, R., Mahalingam, T., Ponnuswamy, V.: Preparation and characterization of electrodeposited SnS thin films. *Optik* **122**, 2216–2219 (2011). <https://doi.org/10.1016/j.ijleo.2011.01.015>
- Minbashi, M., Ghobadi, A., Ehsani, M.H., RezagholipourDizaji, H., Memarian, N.: Simulation of high efficiency SnS-based solar cells with SCAPS. *Sol. Energy* **176**, 520–525 (2018a). <https://doi.org/10.1016/j.solener.2018.10.058>
- Mohan, V.V., Akshaya, K.C., Ashaa, A.S., Jayaraj, M.K., Vijayakumar, K.P.: Effect of substrate temperature on the optoelectronic properties of chemically sprayed SnS thin films. *Mater. Today Proc.* **39**, 1978–1980 (2021). <https://doi.org/10.1016/j.matpr.2020.08.512>
- Movla, H.: Optimization of the CIGS based thin film solar cells: numerical simulation and analysis. *Optik* **125**, 67–70 (2014). <https://doi.org/10.1016/j.ijleo.2013.06.034>
- Nair, P.K., Garcia-Angelmo, A.R., Nair, M.T.S.: Cubic and orthorhombic SnS thin-film absorbers for tin sulfide solar cells. *Phys. Status Solidi (a)* **213**(1), 170–177 (2016). <https://doi.org/10.1002/pssa.201532426>
- Niemegeers, A., Burgelman, M.: Effects of the Au/CdTe back contact on IV and CV characteristics of Au/CdTe/CdS/TCO solar cells. *J. Appl. Phys.* **81**, 2881–2886 (1997). <https://doi.org/10.1063/1.363946>
- Niemegeers, A., Burgelman, M.: Numerical modelling of ac-characteristics of CdTe and CIS solar cells. In: Photovoltaic Specialists Conference, 1996, Conference Record of the Twenty Fifth IEEE, pp. 901–904. IEEE (1996)
- Niemegeers, A., Gillis, S., Burgelman, M.: A user program for realistic simulation of polycrystalline hetero-junction solar cells: SCAPS-1D. In: Proceedings of the 2nd World Conference on Photovoltaic Energy Conversion. JRC, European Commission, pp. 672–675 (1998). <http://hdl.handle.net/1854/LU-281948>
- Niemegeers, A., Burgelman, M., Decock, K., Verchraeagen, J., Degrave, S.: SCAPS3201 Manual. ELIS, September (2013)

- Ojeda-Barrero, G., Oliva-Avilés, A.I., Oliva, A.I., Maldonado, R.D., Acosta, M., Alonzo-Medina, G.M.: Effect of the substrate temperature on the physical properties of sprayed-CdS films by using an automatized perfume atomizer. *Mater. Sci. Semicond. Process.* **79**, 7–13 (2018). <https://doi.org/10.1016/j.mssp.2018.01.018>
- Robles, V., Trigo, J.F., Guillen, C., Herrero, J.: Growth of SnS thin films by co-evaporation and sulfurization for use as absorber layers in solar cells. *Mater. Chem. Phys.* **167**, 165–170 (2015). <https://doi.org/10.1016/j.matchemphys.2015.10.026>
- Simya, O.K., Mahaboobatcha, A., Balachander, K.: A comparative study on the performance of Kesterite based thin film solar cells using SCAPS simulation program. *Superlattices Microstruct.* **82**, 248–261 (2015). <https://doi.org/10.1016/j.spmi.2015.02.020>
- Sinsersuksakul, P., Sun, L., Lee Sang, W., Park Helen, H., Kim Sang, B., Yang, C., Gordon Roy, G.: Overcoming efficiency limitations of SnS-based solar cells. *Adv. Energy Mater.* **4**, 1400496 (2014). <https://doi.org/10.1002/aenm.201400496>
- Son, M.Y., Kim, J.H., Kang, Y.C.: Study of Co<sub>3</sub>O<sub>4</sub> mesoporous nanosheets prepared by a simple spray-drying process and their electrochemical properties as anode material for lithium secondary batteries. *Electrochim. Acta* **116**, 44–50 (2014). <https://doi.org/10.1016/j.electacta.2013.10.217>
- Thangaraju, B., Kaliannan, P.: Spray pyrolytic deposition and characterization of SnS and SnS<sub>2</sub> thin films. *J. Phys. D Appl. Phys.* **33**, 1054–1059 (2000). <https://doi.org/10.1088/0022-3727/33/9/304>
- Wang, W., Winkler, M.T., Gunawan, O., Gokmen, T., Todorov, T.K., Zhu, Y., Mitzi, D.B.: Device characteristics of CZTSSe thin-film solar cells with 12.6% efficiency. *Adv. Energy Mater.* **4**, 1–5 (2014). <https://doi.org/10.1002/aenm.201301465>
- Wang, L.K., Chen, J.J., Yu, J.Y., Zhao, H.L., Yang, J.K.: Highly textured spray-deposited SnO<sub>2</sub>: F films with high haze for solar cells. *Vacuum* **169**, 108879 (2019). <https://doi.org/10.1016/j.vacuum.2019.108879>
- Zhu, J., Wang, D., Liu, T.: One-pot synthesis of SnS nanorods and their lithium storage properties. *Ionics* **20**(1), 141–144 (2014). <https://doi.org/10.1007/s11581-013-1018-7>

**Publisher's Note** Springer Nature remains neutral with regard to jurisdictional claims in published maps and institutional affiliations.

Springer Nature or its licensor (e.g. a society or other partner) holds exclusive rights to this article under a publishing agreement with the author(s) or other rightsholder(s); author self-archiving of the accepted manuscript version of this article is solely governed by the terms of such publishing agreement and applicable law.